The role of the focusing field profile on the stability of periodically focused particle beams

J. S. Moraes, F. B. Rizzato, and R. Pakter

Citation: Physics of Plasmas **10**, 4811 (2003); doi: 10.1063/1.1619139
View online: http://dx.doi.org/10.1063/1.1619139
View Table of Contents: http://scitation.aip.org/content/aip/journal/pop/10/12?ver=pdfcov
Published by the AIP Publishing

The role of the focusing field profile on the stability of periodically focused particle beams

J. S. Moraes
Instituto de Física, Universidade Federal do Rio Grande do Sul, Caixa Postal 15051, 91501-970 Porto Alegre, RS, Brazil
and Centro Universitário La Salle, Av. Victor Barreto, 2288, 92010-000, Canoas, RS, Brazil

F. B. Rizzato and R. Pakter[a)]
Instituto de Física, Universidade Federal do Rio Grande do Sul, Caixa Postal 15051, 91501-970 Porto Alegre, RS, Brazil

(Received 23 May 2003; accepted 25 August 2003)

In this paper, the role of the focusing field profile on the stability of periodically focused particle beams is investigated, paying special attention to the transport within the new regions of stability found recently for vacuum-phase advances well above 90° [R. Pakter and F. B. Rizzato, Phys. Rev. Lett. **87**, 044801 (2001)]. In particular, a solenoidal focusing field profile that goes from a smooth sinusoidal-like function to a sharp-edged step-funcion as a continuous parameter is varied is considered. It is shown that the new regions are always present, but may be very sensitive to changes in the focusing field profile. Specifically, as the focusing field becomes more localized, the new regions become narrower, occur at higher vacuum phase advances, and present a larger number of nonlinear resonances and chaos in the beam envelope phase space. Although in all the cases analyzed here it was found that there is a relatively thick layer of regular trajectories isolating the matched solution from the chaotic region, self-consistent simulations show that envelope phase-space chaos may affect beam dynamics, leading to some small emittance growth. © *2003 American Institute of Physics.* [DOI: 10.1063/1.1619139]

I. INTRODUCTION

The physics of intense beams in periodically focusing systems is an active area of theoretical and experimental research where one looks for external field configurations capable of confining high-current, low emittance ion or electron beams.[1–5] The area is crucial for the development of several advanced particle accelerator applications such as tritium production, spallation neutron source, heavy ion fusion, coherent radiation sources, and nuclear waste transmutation,[6] as well as applications in basic science.

A key aspect of periodically focused beams is their equilibrium and stability properties. Equilibria are obtained when the focusing forces imposed by the confining magnetic field and the self-current balance the defocusing forces due to electrostatic, thermal and beam rigid rotation effects in such a way that the beam transverse radius oscillates with the same periodicity of the focusing field. These solutions are called the *matched solutions*. Until recently, it was believed that only one matched solution is present for a given set of beam and focusing parameters and that this solution becomes unstable as the focusing field intensity is raised above a certain threshold.[2,7–9] The threshold corresponds to a vacuum-phase advance of 90°. By *vacuum-phase advance* we mean the angle that a particle would rotate per focusing period in the presence of the external field but in the abscence of space-charge, and is used here as a measure of the focusing magnetic field strength. Recently, however, it was shown that new regions of stability that lead to much tighter beam confinement are present for focusing fields corresponding to vacuum-phase advances well above 90°.[10] In fact, the scenario as the focusing field increases is the appearance of successive regions of stability which are interrupted by gaps where either the matched solutions are unstable or simply do not exist. Detailed analysis on the effects of beam intensity revealed that, although presenting some different characteristics regarding the bifurcations of the matched solutions, the new regions of stability are present for both emittance-dominated and space-charge-dominated beams.[11] The dynamical mechanism responsible for the onset of the gaps is analyzed in Ref. 12.

Even though all the analysis done so far on the new regions of stability considered a particular focusing field profile, namely a sinusoidal-like profile, it suggests that the onset of the new matched solutions may be highly dependent on the oscillatory components of the field. In the sinusoidal case, for instance, we see that the larger the amplitude of oscillation, the larger the instability gaps.[10,11] Other models analyze different field profiles but in the abscence of space-charge.[13] Given that and the fact that in many experiments, due to engineering and design issues, the magnetic field is more localized, presenting sharper edges and vanishingly small values at sizable fractions of the periodic cell, an important issue to be addressed is the precise role played by the focusing field profile on the stability of periodically focused particle beams.

In this paper, we perform a detailed investigation of

a)Electronic mail: pakter@if.ufrgs.br

beam envelope stability for a more general periodic focusing field profile, which may describe more accurately a broader range of realistic system configurations. In particular, we consider a high-current beam in a periodic solenoidal focusing field whose profile goes from a smooth sinusoidal-like function to a sharp-edged step-funcion as a continuous paramenter is varied. It is shown that the new regions are always present, irrespective to the specific field profile. However, in contrast to the original region of stability, which is in general not greatly affected by the field profile, the new regions do depend on the specific field shape. In particular, the new regions become narrower and occur at higher vacuum phase advances as the focusing field becomes more localized. Due to the increase in the Fourier spectral content of a focusing field profile with sharper edges, the envelope phase-space is also affected presenting a larger number of nonlinear resonances and chaos. Although in all the cases analyzed here we found that there is a relatively thick layer of regular trajectories surrounding the matched solution, isolating it from the chaotic region, self-consistent simulations show that envelope phase-space chaos may affect beam dynamics, leading to some small emittance growth.

The work is organized as follows: in Sec. II we introduce the model with the more general focusing field profile considered; in Sec. III we analyze beam transport stability as a function of the focusing field profile, paying special attention to the new regions of stability and in Sec. IV we conclude the work.

II. THE MODEL

We consider a thin, continuous beam propagating with average axial velocity $\beta_b c\hat{\mathbf{e}}_z$ through a periodic solenoidal focusing magnetic field described by

$$\mathbf{B}(x,y,s)=B_z(s)\hat{\mathbf{e}}_z-\tfrac{1}{2}B_z'(s)(x\hat{\mathbf{e}}_x+y\hat{\mathbf{e}}_y), \tag{1}$$

where $s=z/S=\beta_b ct/S$ is the dimensionless coordinate along the beam axis, $B_z(s+1)=B_z(s)$ is the periodic magnetic field on the beam axis, the prime denotes derivative with respect to s, c is the speed of light *in vacuo*, and S is the periodicity length of the magnetic focusing field. In the paraxial approximation the envelope equation that dictates the envelope evolution of a particle beam in the focusing magnetic field given by Eq. (1) is, in its dimensionless form

$$\frac{d^2r_b}{ds^2}+\kappa_z(s)r_b-\frac{K}{r_b}-\frac{1}{r_b^3}=0. \tag{2}$$

In Eq. (2), $r_b(s)=r_{b_{\text{dimensional}}}/(S\epsilon)^{1/2}$ is the normalized beam envelope radius and $K=2q^2N_bS/\epsilon\gamma_b^3\beta_b^2mc^2$ is the normalized perveance of the beam where ϵ is the unnormalized emittance of the beam, N_b is the number of particles per unit axial length, and q, m, and $\gamma_b=(1-\beta_b^2)^{-1/2}$ are, respectively, the charge, mass, and relativistic factor of the beam particles. The focusing field is characterized by the normalized focusing strength parameter $\kappa_z(s+1)=\kappa_z(s)$ related to the magnetic field by $\kappa_z(s)=q^2B_z^2(s)S^2/4\gamma_b^2\beta_b^2m^2c^4$.

In order to investigate the role of the focusing field profile on beam transport, we consider a focusing field parameter of the form

$$\kappa_z(s)=\sigma_0^2\left[\frac{1+\cos\theta(s)}{N}\right], \tag{3}$$

with the phase function given by

$$\theta(s)=\pi\left\{\frac{\tan^{-1}[\Delta(\bar{s}+\eta/2)]+\tan^{-1}[\Delta(\bar{s}-\eta/2)]}{\tan^{-1}[\Delta(1+\eta)/2]+\tan^{-1}[\Delta(1-\eta)/2]}\right\}, \tag{4}$$

where $\sigma_0=[\int_0^1\kappa_z(s)ds]^{1/2}$ is the vacuum phase advance in the smooth-beam approximation, which is proportional to the rms focusing field, $N=1+\int_0^1\cos\theta(s)ds$ is used to normalize the function, $\bar{s}=\mathrm{mod}(s+1/2,1)-1/2$ is periodic in s and lies always in the range $-1/2\leqslant\bar{s}\leqslant 1/2$, $\Delta>0$ is the focusing field profile paramenter, and $0<\eta\leqslant 1$ is the filling factor. The function $\kappa(s)$ in Eq. (3) is constructed such that for small Δ it resembles a smooth sinusoidal function of period 1 in s, while for increasing Δ it starts developing sharper edges, eventually turning into a discontinuous periodic step function of filling factor η for infinite Δ. In fact, in the limit $\Delta\ll 1$ the arguments of the inverse tangent functions in Eq. (4) are small, allowing the approximation $\tan^{-1}(x)=x$ which leads to $\theta(s)=2\pi\bar{s}$ and to the sinusoidal focusing field profile

$$\kappa_z(s)=\sigma_0^2[1+\cos(2\pi s)], \tag{5}$$

studied in Refs. 10 and 11. Note that in this limit, η plays no role in focusing field profile. On the other hand, when $\Delta\gg 1$ the inverse tangent functions present an abrupt change from $-\pi/2$ to $\pi/2$ as their arguments change sign, allowing the approximation $\tan^{-1}(x)=(\pi/2)\mathrm{sign}(x)$ which leads to a discontinuous phase function with $\theta(\bar{s}<-\eta/2)=-\pi$, $\theta(-\eta/2<\bar{s}<\eta/2)=0$ and $\theta(\bar{s}>\eta/2)=\pi$, and to the step-function focusing field lattice with filling factor η,

$$\kappa_z(s)=\begin{cases}0, & \eta/2<s<1-\eta/2\\ \sigma_0^2/\eta, & \text{otherwise.}\end{cases} \tag{6}$$

Note that for all Δ, the denominator in Eq. (4) guarantees that the phase function completes a full cycle from $\theta=-\pi$ to $\theta=\pi$ as $\bar{s}$ goes from $-1/2$ to $1/2$, and consequently $\kappa_z(s)$ is always continuous at the lattice boundaries.

It is worth pointing out that the static magnetic field in Eq. (1) must satisfy the Maxwell's equations $\nabla\cdot\mathbf{B}=0$ and $\nabla\times\mathbf{B}=0$. While the first equation is exactly satisfied, the second one is valid only if we assume that the transverse beam envelope is much smaller than the typical length of variation of B_z along the beam axis, such that $r_b^nB_z^{(n)}/B_z\ll 1$, where $B_z^{(n)}\equiv d^nB_z/ds^n$, and terms of order $n\geqslant 2$ are neglected. This assumption is certainly not true as $\Delta\to\infty$ and the field profile tends to the sharp-edged step-function of Eq. (6). Therefore, although the step-function lattice is widely used to model periodic focusing fields, it is important to keep in mind that real focusing channels have a smooth $\kappa_z(s)$ which is more properly represented by a finite Δ.

To illustrate the focusing field profiles in Eq. (3), Fig. 1 shows $\kappa(s)$ for $\eta=0.2$, $\sigma_0=70°$ and four different values of Δ: 10^{-1}, 10^1, 10^2, and 10^4. It is clear that as Δ increases, the focusing field becomes more localized with sharper edges, being very simililar to the step-function focusing lattice for $\Delta=10^4$. Moreover, comparing the phase function $\theta(s)$ for

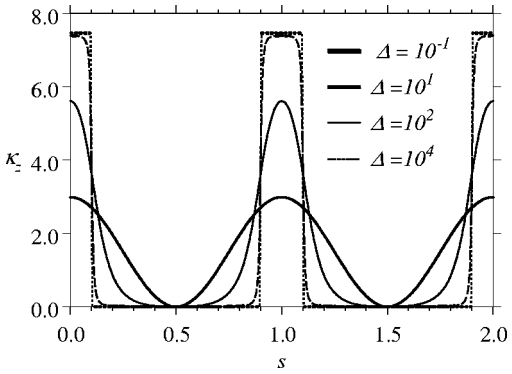

FIG. 1. Focusing field profile $\kappa_z(s)$ for different values of the parameter Δ. The other parameters are $\eta=0.2$ and $\sigma_0=70°$.

the profile obtained with $\Delta=10^{-1}$ with that of the sinusoidal function $\theta(s)=2\pi s$ we found that they differ by less than 0.1% for all s.

III. BEAM STABILITY ANALYSIS

A. Envelope equation analysis

In this section, we analyze the stability of beams propagating through the focusing field given in Eq. (3), as the focusing field profile is varied. We pay special attention to the new regions of stability found in Refs. 10 and 11. To perform the analysis we use a Newton–Raphson method to search for and verify the stability of envelope matched solutions obtained from Eq. (2). The Newton–Raphson method applied to the current envelope problem is described in detail in the Appendix. The stability is determined with the aid of the stability index α defined as $\alpha=\cos(k_{\mathrm{fix}})$, where k_{fix} is the wave number of small linear oscillations around the periodic trajectory, obtained with the Newton–Raphson method. For stable orbits where k_{fix} is a real number, $|\alpha|<1$; if α crosses the lower boundary $\alpha=-1$ it undergoes a period doubling bifurcation loosing stability, and if the orbit crosses the upper boundary $\alpha=+1$ the orbit undergoes an inverse tangent bifurcation with a previous unstable fixed point. In order to gather some information on the nonlinear stability of the matched solutions, we also make use of Poincaré plots of the envelope phase-space. The plots are obtained by integrating the envelope equation (2) and recording the pair $(r_b, dr_b/ds)$ every period of the external focusing field at integer values of s.[14]

Generally, the bifurcation scenario for the matched solutions as one increases the vacuum phase advance is as follows; a detailed description is found in Refs. 10 and 11. Stable matched solutions are born in the phase space with $\alpha=+1$. For the original matched solution, this occurs exactly at $\sigma_0=0°$, whereas for the new regions of stability it occurs at different $\sigma_0>180°$. As the vacuum phase advance is increased, the respective α moves towards $\alpha=-1$. When $\alpha=-1$ is reached, the matched solution suffers a period doubling bifurcation and becomes unstable. We define as a region of stability, the range of σ_0 that goes from the onset of the corresponding stable matched solution with $\alpha=+1$ until it bifurcates with $\alpha=-1$. As a matter of fact, before eventually disappearing permanently from the phase space, the matched solutions cross back the $\alpha=-1$ line and recover their stability as σ_0 is further increased. However, as shown in Ref. 11 the matched solution is not useful for beam confinement after its restabilization because beam emittance growth was observed in self-consistent numerical simulations for these parameter regions.

In harmonic cases where the confining magnetic field oscillates sinusoidally, the following series of analytic results were obtained.[11,12] The new regions of stability occurs when the oscillatory frequency of the magnetic field matches the frequency with which the envelope itself oscillates. This frequency matching may take place in virtue of the fact that while the magnetic field has indeed a fixed frequency, the envelope frequency varies over a range of values determined by all the control parameters of the system. In particular, the envelope frequency increases with the magnetic field intensity and has an approximate value $2\sigma_0$. Since the magnetic field frequency is 2π, one concludes that the second region approximately lies in the parametric region determined by $2\sigma_0\sim 2\pi$, or $\sigma_0\sim 180°$.[10] More precise calculations based on normal forms of bifurcation theory were extensively developed in Refs. 12 and 11 and actually show that after a parametric gap where no matched solution is present is cleared, the second region is formed when σ_0 actually becomes larger than 180°. In harmonic cases the size of the gap along the σ_0 axis is roughly given by 180°.

In the general case of anharmonic confining fields, numerical analysis is needed but we observe that the basic results still hold except perhaps for the fact that the gaps may become larger, as investigated in what follows.

To determine the role of the focusing field profile on the beam transport stability we construct a parametric space plot of $\sigma_0\times\Delta$ displaying the locations of the different regions of stability. Recalling from Sec. I, Δ determines the overall shape of the focusing field: as Δ is increased from small values $\Delta\ll 1$, the focusing field profile continuously goes from a smooth sinusoidal function to a sharp-edged step-function as $\Delta\to\infty$. In the plots we use a Newton–Raphson method to numerically determine the boundaries $\sigma_0=\sigma_0(\Delta)$ where stable matched solutions emerge in the phase space with $\alpha=+1$ and lose stability with $\alpha=-1$. The results for the first two regions of stability (the original and its first neighbor) obtained for $\eta=0.5$ (a) and $\eta=0.2$ (b) are shown in Fig. 2, where the beam intensity is chosen to be $K=5.0$. The black regions correspond to stable regions; the region below $\sigma_0\approx 100°$ is the original region of stability (ORS) and the other one is the second region of stability (SRS). Higher order new regions of stability were also investigated and the results are qualitatively the same as for the SRS.

For the larger filling factor case $\eta=0.5$, Fig. 2(a) shows that the regions of stability are not greatly affected by the variations in Δ. Only some narrowing of the SRS is noticed as the focusing field becomes more localized (increasing Δ). Panels (a) and (b) of Fig. 3 compare Poincaré plots of the phase space for the SRS obtained for the limiting cases $\Delta=10^{-1}$ and $\Delta=10^{4}$ of Fig. 2(a). In order to compare matched solutions with similar stability features, we consider

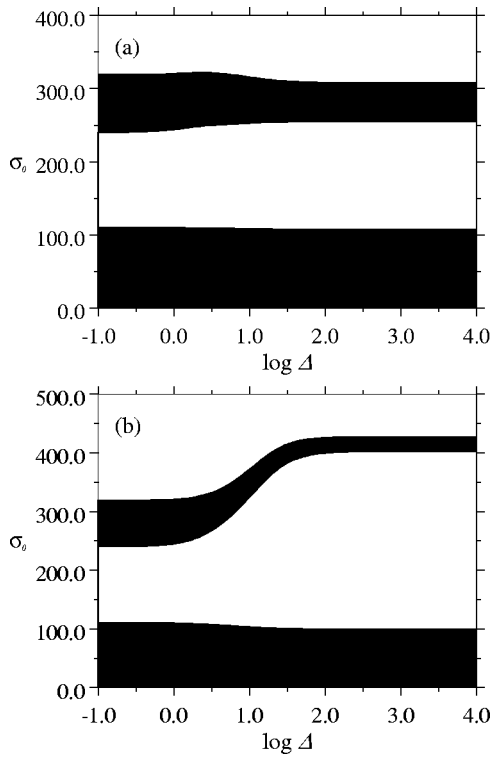

FIG. 2. Parametric space plots $\sigma_0 \times \Delta$ showing the location of the first two regions of stability for (a) $\eta = 0.5$ and (b) $\eta = 0.2$. The beam intensity corresponds to $K = 5.0$.

vacuum phase advances that lead to the same stability index α in both cases. In particular, we choose $\alpha = -0.58$ which leads to $\sigma_0 = 297.3°$ for $\Delta = 10^{-1}$ and $\sigma_0 = 294.2°$ for $\Delta = 10^4$. It is seen that while for the $\Delta = 10^{-1}$ case the phase space is completely regular, for the $\Delta = 10^4$ case the increase in the number of significant focusing field profile Fourier components is responsible for the onset of resonant islands in the phase space. However, in this case the resonances are small, leading to neither overlap nor chaos, and occur far from the matched solution. This suggests that they are relevant only for very mismatched beams. Therefore, for such *large* filling factor, one may conclude that the exact shape of the focusing field is not critical for beam stability.

On the other hand, for the smaller filling factor case $\eta = 0.2$ shown in Fig. 2(b), the focusing field profile plays an important role in the beam stability and as Δ increases two effects are clearly seen regarding the SRS. (i) First, there is an increase in the vacuum phase advance necessary to reach the SRS. Since σ_0 is proportional to the rms focusing field, this reveals that the peak magnetic field has to be raised considerably as the profile becomes more localized with *small* η not only because its average has to increase, but also because the spatial region where the field is effectively applied is smaller. In the case depicted in Fig. 2(b), for instance, taking into account that σ_0 for the SRS increases roughly 50% as Δ goes from 10^{-1} to 10^4, the increase in the peak magnetic field has to be about 3.75 times. However, if one now looks at the minimum value attained by the matched beam envelope as it oscillates in the focusing lattice—we call it r_b^*, an important quantity since we are interested in beams with the smallest possible transverse dimensions—one notes that as the peak magnetic field for the SRS increases with Δ, r_b^* is noticeably reduced. Figure 4 presents r_b^* vs $\log \Delta$ and shows that the decrease in r_b^* as Δ goes from 10^{-1} to 10^4 is about 5 times which in fact exceeds the increase in the peak magnetic field intensity. (ii) Second, the SRS becomes much narrower as Δ is increased. The range in vacuum phase advance for which the SRS exists goes from 80° to 25° as Δ is increased. Not only this reveals that a more accurate field intensity tuning is necessary as the focusing channel becomes more localized for $\eta = 0.2$, but it also suggests that more nonlinear resonances may appear in the phase space because the variation of α with σ_0, and hence the range of orbital frequencies in the phase space, is larger. This is confirmed by the Poincaré plots of the phase space for the SRS shown in Figs. 3(c)–3(f), with $\Delta = 10^{-1}$, 10^1, 10^2, and 10^4, respectively, which correspond to the same values of Δ used in Fig. 1. Again, to compare cases with similar stability features, in all the panels the vacuum phase advance is chosen such that the stability factor is always $\alpha = -0.58$. In panel (c) ($\Delta = 10^{-1}$), the phase space is completely regular with the absence of nonlinear resonances and chaos. As Δ is increased to 10^1 [panel (d)], several groups of nonlinear resonances emerge. However, they are still small such that neither resonance overlap nor chaos is noticeable. Increasing Δ even further to 10^2 [panel (e)], the nonlinear resonant islands grow considerably with more apparent separatrix chaos and resonance overlap. For $\Delta = 10^4$ [panel (f)] the resonant islands are fully overlapped presenting a thick chaotic layer which seems to form an extented chaotic region along which the beam envelope can diffuse to higher and higher values as the mismatched beam propagates. Although in all the cases presented in Figs. 3(c)–3(f) there is always a relatively thick layer of regular trajectories surrounding the matched solution, isolating it from any chaos that may be present, chaos in the envelope phase space may still affect beam transport, leading to beam quality loss as suggested in Ref. 9. This issue will be studied in more detail in the following subsection with the aid of self-consistent beam simulation.

Other values of the filling factor η were also investigated and the overall conclusion is that $\eta = 0.5$ may be seen as a midpoint in the sense that, as shown for the SRS above, at this value the new regions of stability are not greatly affected by the variations in the focusing field profile parameter. This is probably connected to the fact that exactly at $\eta = 0.5$ the sinusoidal ($\Delta \to 0$) and the step-function ($\Delta \to \infty$) limits of the focusing profile present the same norm $N = 1 + \int_0^1 \cos\theta(s) ds = 1.0$, such that the peak magnetic field is the same in both cases. For $\eta > 0.5$ it was found that the new regions tend to increase in size as Δ is increased from 0, getting closer to the ORS. In fact, one may eventually find parameter sets for which two stable matched solutions coexist in the phase space. On the other hand, as shown in detail for $\eta = 0.2$, when $\eta < 0.5$ the new regions become narrower and occur at higher vacuum phase advances as Δ is increased. In particular, for the thin lens regime where $\eta \to 0$, $\Delta \to \infty$, and $\kappa_z(s)$ tends to a series of Dirac-delta functions, the onset of the new regions of stability only occur at σ_0

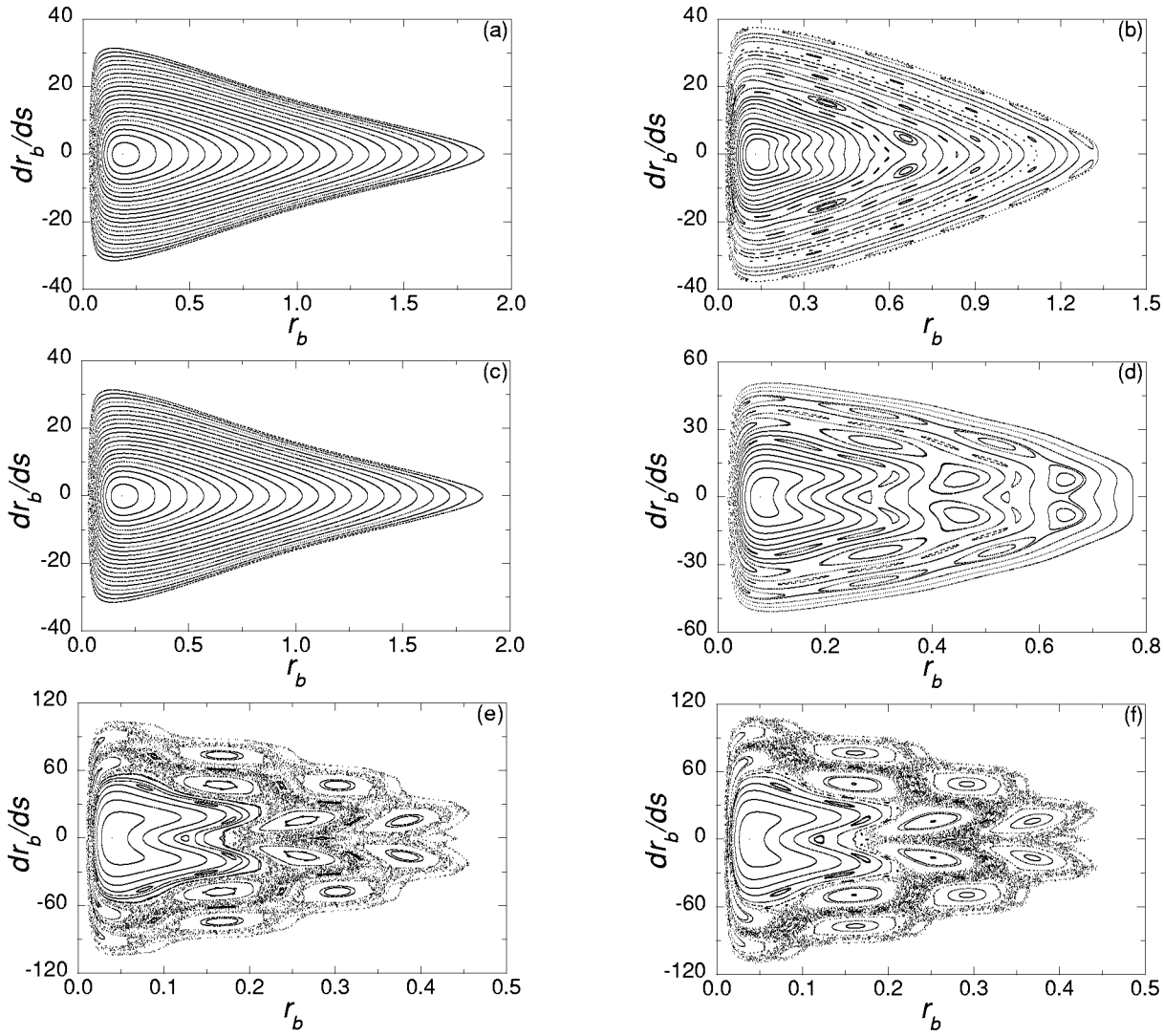

FIG. 3. Poincaré plots of the r_b vs dr_b/ds phase space for $K=5.0$ and (a) $\eta=0.5$, $\Delta=10^{-1}$, $\sigma_0=297.3°$; (b) $\eta=0.5$, $\Delta=10^4$, $\sigma_0=294.2°$; (c) $\eta=0.2$, $\Delta=10^{-1}$, $\sigma_0=297.3°$; (d) $\eta=0.2$, $\Delta=10^1$, $\sigma_0=357.9°$; (e) $\eta=0.2$, $\Delta=10^2$, $\sigma_0=418.4°$; (f) $\eta=0.2$, $\Delta=10^4$, $\sigma_0=420.2°$. All the cases correspond to the SRS with the same stability index $\alpha=-0.58$.

$\rightarrow\infty$, which in practice means that these regions are absent. However, as discussed in Sec. II, this limit is not realistic due to the restrictions imposed by Maxwell's equations on the focusing field given by Eq. (1).

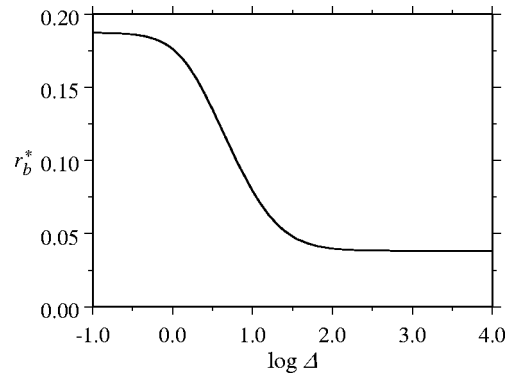

FIG. 4. The minimum oscillatory radius of stable matched solutions r_b^* as a function of Δ for the SRS with $\eta=0.2$, $K=5.0$, and $\alpha=-0.58$.

B. Self-consistent numerical beam simulation

To further investigate beam transport stability we also perform self-consistent numerical simulations using the Green's function method with finite size macroparticles[15] to compute the self-fields. In the simulations $N=2500$ macroparticles are launched according to the Kapchinskij–Vladimirskij distribution[1] and are transported along the focusing field profile given in Eq. (3). The finite number of macroparticles naturally introduces envelope mismatch and beam distribution imprecisions which act as the seed for any possible instability to develop. As the beam propagates, we compute the self-consistently obtained KV beam radius

$$r_b=(2\langle x^2+y^2\rangle)^{1/2}, \tag{7}$$

which is $\sqrt{2}$ the rms radius, and the rms transverse emittances

$$\epsilon_\zeta=4[\langle\zeta^2\rangle\langle\zeta'^2\rangle-\langle\zeta\zeta'\rangle^2]^{1/2}, \quad \zeta=x,y \tag{8}$$

to determine if beam quality is preserved. In Eqs. (7) and (8), $\langle\cdots\rangle$ represents an average over macroparticles.

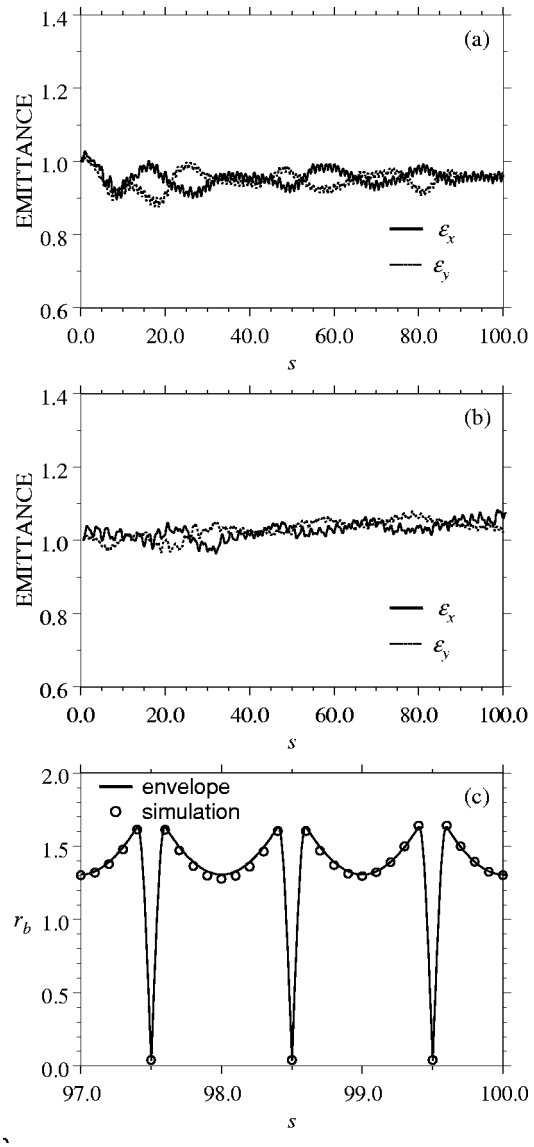

FIG. 5. In panels (a) and (b), rms transverse emittances ϵ_x and ϵ_y vs s obtained via self-consistent numerical simulation for the same parameters as in Figs. 3(c) and 3(f), respectively. In panel (c) comparison of beam radius results obtained from the envelope equation (2) and the self-consistent simulations for the last 3 periods of the run presented in panel (b).

In Fig. 5 we compare emittance evolution for the cases corresponding to those shown in panels (c) and (f) of Fig. 3. One notes that while in the quasi-sinusoidal case $\Delta = 10^{-1}$ of Fig. 5(a) emittance remains leveled at $\epsilon_{x,y} = 1$, in the quasi-sharp-edged case $\Delta = 10^4$ there is a slight growth. The growth is probably associated with the presence of nonlinear resonances seen in Fig. 3(f), as suggested in Ref. 9, but is not strong enough to destabilize the envelope dynamics. In fact, the last panel, Fig. 5(c), shows that the agreement between the envelope dynamics obtained from self-consistent simulations and from Eq. (2) (which assumes constant emittance) is preserved throughout the focusing channel. Emittance growth, even small as the case here, is always a troubling factor in beam tranport. However, the disadvantage it brings to beam control may be compensated by the tighter radii obtained in the SRS, all depending on the experimental conditions and purposes. In any case, emittance growth is expected to be smaller than the quasi-sharp-edged case examined here given the relative smoothness of realistic field configurations.

IV. CONCLUSIONS

To conclude, we have performed a detailed stability analysis of periodically focused particle beams propagating through generic focusing field profiles, which may describe more accurately a broader range of realistic system configurations. Special attention was given to transport within the new regions of stability found recently for vacuum-phase advances well above 90°.[10,11] In particular, we considered a high-current beam in a periodic solenoidal focusing field whose profile goes from a smooth sinusoidal-like function to a sharp-edged step-funcion as a continuous parameter is varied. It was shown that the new regions are always present, irrespective to the specific field profile. However, in contrast to the original region of stability, which is in general not greatly affected by the field profile, the new regions do depend on the particular field shape. Specifically, the new regions become narrower and occur at higher vacuum phase advances as the focusing field becomes more localized. Due to the increase in the Fourier spectral content of a focusing field profile with sharper edges, the envelope phase-space is also affected presenting a larger number of nonlinear resonances and chaos. Although in all the cases analyzed here we found that there is a relatively thick layer of regular trajectories surrounding the matched solution, isolating it from the chaotic region, self-consistent simulations showed that envelope phase-space chaos may affect beam dynamics, leading to some small emittance growth.

ACKNOWLEDGMENT

This work was supported by CNPq, Brazil.

APPENDIX: NEWTON–RAPHSON METHOD FOR MATCHED SOLUTIONS

The evolution of the envelope in the $[r_b, r_b']$ phase space is dictated by the normalized envelope equation (2), which can be writen in the equivalent form

$$\frac{d\mathbf{X}}{ds} = \mathbf{F}(\mathbf{X}, s), \tag{A1}$$

where $\mathbf{X} \equiv [r_b, r_b']$ is the position vector in the phase space and $\mathbf{F}(\mathbf{X}, s) = [r_b', -\kappa_z(s) r_b + K/r_b + 1/r_b^3]$. To apply the Newton–Raphson method to search for and verify the stability of envelope matched solutions we consider the mapping function $\mathbf{\Phi}$ which maps the envelope phase space onto itself every period of the focusing field. Formally, the mapping may be expressed as

$$\mathbf{X}(s_0 + 1) = \mathbf{\Phi}[\mathbf{X}(s_0)], \tag{A2}$$

where s_0 is an initial position in the focusing lattice. In this context a matched solution $\mathbf{X}_m$ corresponds to a fixed point of the mapping that satisfies

$$\mathbf{X}_m = \mathbf{\Phi}[\mathbf{X}_m]. \tag{A3}$$

Let us suppose that we know a guess solution $\mathbf{X}_g$ that is close to a matched solution such that

$$\mathbf{X}_m = \mathbf{X}_g - \delta\mathbf{X} \tag{A4}$$

with $\delta\mathbf{X}$ *small*. Substituting Eq. (A4) in Eq. (A3) and Taylor expanding up to linear terms in $\delta\mathbf{X}$ we obtain

$$\{\delta\mathbf{\Phi}[\mathbf{X}_g] - \mathbf{I}\}\delta\mathbf{X} = \mathbf{X}_g(s_0+1) - \mathbf{X}_g(s_0), \tag{A5}$$

where

$$\delta\mathbf{\Phi} = \begin{bmatrix} \partial r_b(s_0+1)/\partial r_b(s_0) & \partial r_b(s_0+1)/\partial r_b'(s_0) \\ \partial r_b'(s_0+1)/\partial r_b(s_0) & \partial r_b'(s_0+1)/\partial r_b'(s_0) \end{bmatrix} \tag{A6}$$

is the tangent mapping matrix and $\mathbf{I}$ is the 2×2 identity matrix. The Newton–Raphson method consists of, given an initial guess for the matched solution $\mathbf{X}_g$ and integrating the appropriate differential equations over one period of focusing field, solve for $\delta\mathbf{X}$ in Eq. (A5) and use this result in Eq. (A4) to obtain a new approximation to the matched solution $\mathbf{X}_m$. After iterating this process many times, the solution may converge to a given matched solution of the system. Once convergence is reached, $\delta\mathbf{\Phi}$ becomes the matrix that descrides the evolution (mapping) of infinitesimal perturbations around the matched solution, and therefore has information on the stability of the matched solution. In particular, if $|\mathrm{Trace}[\delta\mathbf{\Phi}]| > 2$, its eigenvalues are real and the matched solution is an unstable saddle point—note that the envelope equation (A1) is conservative such that $\det[\delta\mathbf{\Phi}] = 1$—on the other hand, if $|\mathrm{Trace}[\delta\mathbf{\Phi}]| < 2$ the eigenvalues are complex on the form $\exp(ik_{\mathrm{fix}})$ and $\exp(-ik_{\mathrm{fix}})$ and the surrounding orbits rotate with wave number k_{fix} around the stable matched solution. The stability index is coveniently defined as $\alpha = (1/2)\mathrm{Trace}[\delta\mathbf{\Phi}]$.

In principle, matrix $\delta\mathbf{\Phi}$ can be evaluated *directly* by numerically computing approximations to the derivatives on the right-hand side of Eq. (A6). However a more accurate method which was used here can be derived from the envelope equation (A1). Namely, after some straightforward calculations we can show that $\delta\mathbf{\Phi} = \mathbf{A}(s_0+1)$, where $\mathbf{A}(s)$ is a matrix whose elements are continuous functions of s, obtained by integrating along with Eq. (A1) the equation

$$\frac{d\mathbf{A}}{ds} = \frac{d\mathbf{F}}{d\mathbf{X}} \cdot \mathbf{A}, \tag{A7}$$

using as initial condition $\mathbf{A}(s_0) = \mathbf{I}$. In Eq. (A7), $d\mathbf{F}/d\mathbf{X}$ is the Jacobian matrix of $\mathbf{F}(\mathbf{X}, s)$.

[1] I. M. Kapchinskij and V. V. Vladimirskij, in *Proceedings of the International Conference on High Energy Accelerators* (CERN, Geneva, 1959), p. 274.
[2] I. Hofmann, L. J. Laslett, L. Smith, and I. Haber, Part. Accel. **13**, 145 (1983).
[3] R. C. Davidson, *Physics of Non-Neutral Plasmas* (Addison–Wesley, Reading, 1990).
[4] M. Reiser, *Theory and Design of Charged-Particle Beams* (Wiley, New York, 1994).
[5] C. Chen, R. Pakter, and R. C. Davidson, Phys. Rev. Lett. **79**, 225 (1997).
[6] See, e.g., *Space Charge Dominated Beams and Applications of High-Brightness Beams*, edited by S. Y. Lee, AIP Conf. Proc. No. **377** (AIP, New York, 1996).
[7] P. M. Lapostolle, IEEE Trans. Nucl. Sci. **NS-18**, 1101 (1971); F. J. Sacherer, *ibid.* **NS-18**, 1105 (1971).
[8] C. J. Struckmeier and M. Reiser, Part. Accel. **14**, 227 (1984).
[9] C. Chen and R. C. Davidson, Phys. Rev. Lett. **72**, 2195 (1994); Phys. Rev. E **49**, 5679 (1994).
[10] R. Pakter and F. B. Rizzato, Phys. Rev. Lett. **87**, 044801 (2001).
[11] R. Pakter and F. B. Rizzato, Phys. Rev. E **65**, 056503 (2002).
[12] F. B. Rizzato and R. Pakter, Phys. Rev. Lett. **89**, 184102 (2002).
[13] R. A. Bosch and C. S. Hsue, Chin. J. Phys. (Taipei) **31**, 313 (1993).
[14] A. J. Lichtenberg and M. A. Lieberman, *Regular and Stochastic Motion* (Springer-Verlag, New York, 1992); R. Pakter, G. Corso, T. S. Caetano, D. Dillenburg, and F. B. Rizzato, Phys. Plasmas **1**, 4099 (1994); J. Guckenheimer and P. Holmes, *Nonlinear Oscillations, Dynamical Systems, and Bifurcations of Vector Fields* (Springer-Verlag, New York, 1990).
[15] R. Pakter and C. Chen, Phys. Rev. E **62**, 2789 (2000).